

Projection of Functionals and Fast Pricing of Exotic Options*

Valentin Tissot-Daguette[†]

Abstract

We investigate the approximation of path functionals. In particular, we advocate the use of the Karhunen-Loève expansion, the continuous analogue of Principal Component Analysis, to extract relevant information from the image of a functional. Having accurate estimate of functionals is of paramount importance in the context of exotic derivatives pricing, as presented in the practical applications. In particular, we show how a simulated-based procedure, which we call the Karhunen-Loève Monte Carlo (KLMC) algorithm, allows fast and efficient computation of the price of path-dependent options. We also explore the path signature as an alternative tool to project both paths and functionals.

Keywords — Path functional, Karhunen-Loève expansion, signature, derivatives pricing

MSC (2020) Classification — 91G20, 91G60, 41A45

1 Introduction

The pricing of exotic options remains a difficult task in quantitative finance. The main challenge is to find an adequate trade-off between pricing accuracy and fast computation. Efficient techniques such as finite difference [20] or the fast Fourier transform [6] are in general not applicable to path-dependent payoffs. Practitioners are often forced to turn to standard Monte Carlo methods, despite being slow. Therefore, researchers have come up with novel ideas over the years to tackle this issue. Recently, some authors have employed deep learning to price vanilla and exotic options in a non-parametric manner [5] while others showed the benefits of the path signature [2, 17] to project exotic payoffs in a nonlinear way.

In this paper, we move away from prevailing machine learning methods and bring a classical tool back into play: the Karhunen-Loève (KL) expansion [13, 15]. The latter provides an orthogonal decomposition of stochastic processes that is optimal in the $L^2(\mathbb{Q} \otimes dt)$ sense. The theory has been widely applied to Gaussian processes [10, 21] and recently for the Brownian Bridge in a weighted Hilbert space [8]. In this paper, the KL expansion takes on a newfound importance when it is applied to the projection of path functionals. We propose a simple simulation-based procedure, which we call the Karhunen-Loève Monte Carlo (KLMC) algorithm, to compute the price of exotic options.¹ The superiority of KL-based Monte Carlo methods compared to the ordinary one was shown numerically in [1] for the Brownian case. Our goal is here to further support these findings and extend this approach. We also discuss alternative methods employing the path signature as basis of the space of functionals.

The remainder of this paper is structured as follows. In Section 2, we gather standard results from approximation theory and draw a parallel between Hilbert projection and the à la mode path signature.

*The research has been carried out during Valentin's internship at Bloomberg LP. The author wishes to thank Bruno Dupire for his precious guidance, goodwill and inspiring discussions.

[†]Operations Research and Financial Engineering Department, Princeton University, Princeton, NJ 08544, USA.
Email: v.tissot-daguette@princeton.edu

¹See <https://github.com/valentintissot/KLMC> for an implementation.

Section 3 is devoted to the approximation of functionals, where two routes are contrasted as well as a short discussion on the use of the signature for this task. We apply the developed tools and finally present the KLMC algorithm with accompanying numerical evidence in Section 4.

2 Path Approximation

For fixed horizon $T > 0$, let $\Lambda_t = \mathcal{C}([0, t], \mathbb{R})$ and $\Lambda := \bigcup_{t \in [0, T]} \Lambda_t$. For $X \in \Lambda_t$ and $s \leq t$, X_s denotes the trajectory up to time s , while $x_s = X(s)$ is the value at time s . We equip Λ with a σ -algebra \mathcal{F} , filtration \mathbb{F} and probability measure \mathbb{Q} to form a stochastic basis $(\Lambda, \mathcal{F}, \mathbb{F}, \mathbb{Q})$.

The goal of this paper is to price exotic options with payoff of the form $\varphi = h \circ f$, where $f : \Lambda \rightarrow \mathbb{R}$ is a *functional* and h a real function. For instance, an Asian call option is obtained with $f(X_t) = \frac{1}{t} \int_0^t x_s ds$ and $h(y) = (y - K)^+$. If \mathbb{Q} is a risk-neutral measure and assuming zero interest rate, then

$$p = \mathbb{E}^{\mathbb{Q}}[\varphi(X_\tau)],$$

is the value of the option with payoff φ and maturity $\tau \in [0, T]$. To compute p using Monte Carlo, we typically simulate an approximated version of $X \in \Lambda_\tau$, e.g. using time discretization. Alternatively, we can approximate the *transformed path*,

$$Y = f(X), \quad y_t = f(X_t), \quad t \in [0, \tau],$$

and write $p = \mathbb{E}^{\mathbb{Q}}[h(y_\tau)]$. We favor the second option, as shown throughout the paper and in the numerical experiments.

A natural way to approximate X (or Y) is to project it onto a Hilbert space. For simplicity, we focus on paths defined on the whole interval $[0, T]$, so working on Λ_T is enough. Also, f is assumed to preserve continuity, so $f(X) \in \Lambda_T$ as well. We now present the theory for the original path, although the same would hold for the transformed one; see Section 3. Let \mathcal{H} be a separable Hilbert space with inner product $(\cdot, \cdot)_{\mathcal{H}}$. Then any $X \in \Lambda_T \cap \mathcal{H}$ admits the representation

$$x_t = \sum_k \xi_k F_k(t), \quad \xi_k = (X, F_k)_{\mathcal{H}}, \quad t \in [0, T], \quad (2.1)$$

where $\mathfrak{F} := (F_k)$ is an orthonormal basis (ONB) of \mathcal{H} .² An approximation of X is obtained by truncating the series in (2.1), that is $x_t^{K, \mathfrak{F}} = \sum_{k \leq K} \xi_k F_k(t)$. Each pair (K, \mathfrak{F}) thus induces a projection map $\pi^{K, \mathfrak{F}} : \mathcal{H} \rightarrow \mathcal{H}$ given by $\pi^{K, \mathfrak{F}}(X) = X^{K, \mathfrak{F}}$. Although paths are assumed to be one-dimensional for simplicity, the present framework is easily generalized. Indeed, if $x_t = (x_t^1, \dots, x_t^d) \in \mathbb{R}^d$, it suffices to project each component separately, i.e. $x_t^{i, K, \mathfrak{F}^i} = \sum_{k \leq K} \xi_k^i F_k^i(t)$ with $\xi_k^i = (X^i, F_k^i)_{\mathcal{H}}$ and $(\mathfrak{F}^i)_{i=1}^d$ ONB's of \mathcal{H} .

2.1 Karhunen-Loève Expansion

Let \mathcal{H} be the Lebesgue space $L^2([0, T])$ of square-integrable functions, where we write $(\cdot, \cdot) = (\cdot, \cdot)_{L^2([0, T])}$ for brevity. Among the myriad of bases available, which one should be picked? The answer will depend upon the optimality criterion. One possibility is to minimize the square of the $L^2(\mathbb{Q} \otimes dt)$ -norm (denoted by $\|\cdot\|_*$) between a path and its K -order truncation, i.e.

$$\epsilon^{K, \mathfrak{F}} := \|X - X^{K, \mathfrak{F}}\|_*^2 = \mathbb{E}^{\mathbb{Q}} \int_0^T |x_t - x_t^{K, \mathfrak{F}}|^2 dt,$$

²The enumeration of \mathfrak{F} will depend on its construction and common notations. For instance, \mathfrak{F} may or may not include an initial element F_0 . For fairness sake, however, we always compare projections involving the same number of basis functions.

for $X \in \Lambda_T \cap L^2([0, T])$. Thanks to the orthogonality of \mathfrak{F} , we have

$$\epsilon^{K, \mathfrak{F}} = \sum_{k, l > K} (\xi_k, \xi_l)_{L^2(\mathbb{Q})} (F_k, F_l)_{L^2([0, T])} = \sum_{k > K} \lambda_k^{\mathfrak{F}}, \quad \lambda_k^{\mathfrak{F}} := \|\xi_k\|_{L^2(\mathbb{Q})}^2. \quad (2.2)$$

As the mapping $\mathfrak{F} \mapsto \sum_k \lambda_k^{\mathfrak{F}}$ is constant and equal to the total variance $\|X\|_{L^2(\mathbb{Q} \otimes dt)}^2$, the projection error is solely determined by the speed of decay of $(\lambda_k^{\mathfrak{F}})$. Inversely, the optimal basis will maximize the cumulative sum of variance $\sum_{k \leq K} \lambda_k^{\mathfrak{F}}$. This leads us to the *Karhunen-Loève expansion* [13, 15], the continuous analogue of Principal Component Analysis. In what follows, assume $\mathbb{E}^{\mathbb{Q}}[x_t] = 0 \forall t \in [0, T]$ and define the symmetric kernel $\kappa_X(s, t) = (x_s, x_t)_{L^2(\mathbb{Q})}$. As κ_X is also continuous and non-negative definite, Mercer's representation theorem [18] ensures the existence of an ONB $\mathfrak{F} = (F_k)$ of $L^2([0, T])$ and scalars $\lambda_1^{\mathfrak{F}} \geq \lambda_2^{\mathfrak{F}} \geq \dots \geq 0$ such that

$$\kappa_X(s, t) = \sum_{k=1}^{\infty} \lambda_k^{\mathfrak{F}} F_k(s) F_k(t). \quad (2.3)$$

Then \mathfrak{F} is the *Karhunen-Loève (KL) basis* associated to X under \mathbb{Q} . From (2.3), it is immediate that F_k solves the Fredholm integral equation

$$(\kappa_X(t, \cdot), F_k) = \lambda_k^{\mathfrak{F}} F_k(t), \quad t \in [0, T].$$

Accordingly, \mathfrak{F} and $(\lambda_k^{\mathfrak{F}})$ are termed *eigenfunctions* and *eigenvalues* of κ_X , respectively. Observe that the squared $L^2(\mathbb{Q})$ norm of the KL coefficient $\xi_k = (X, F_k)$ is precisely $\lambda_k^{\mathfrak{F}}$, whence comes the notation in (2.2). The next result reflects the relevance of the KL expansion; see [10, Theorem 2.1.2.] for a proof.

Theorem 2.1. *The Karhunen-Loève basis is the unique ONB of $L^2([0, T])$ minimizing $\epsilon^{K, \mathfrak{F}}$ for all $K \geq 1$.*

Remark 2.2. *For non-centered trajectories, it suffices to characterize the Karhunen-Loève basis of $x_t - \mathbb{E}^{\mathbb{Q}}[x_t]$. The projected path is then obtained by adding the mean function back to the expansion.*

Example 2.3. *Let $T = 1$ and \mathbb{Q} be the Wiener measure, i.e. the coordinate process X is Brownian motion on $[0, 1]$. The covariance kernel is $\kappa_X(s, t) = s \wedge t$, leading to the eigenfunctions $F_k(t) = \sqrt{2} \sin((k-1/2)\pi t)$ and eigenvalues $\lambda_k^{\mathfrak{F}} = \frac{1}{\pi^2(k-1/2)^2}$, $k \geq 1$. For K large enough, the projection error is approximately equal to*

$$\epsilon^{K, \mathfrak{F}} = \frac{1}{\pi^2} \sum_{k > K} \frac{1}{(k-1/2)^2} \approx \frac{1}{\pi^2} \int_K^{\infty} \frac{dk}{(k-1/2)^2} = \frac{1}{\pi^2(K-1/2)}.$$

It is easily seen that $\xi_k = (X, F_k) \sim \mathcal{N}(0, \lambda_k^{\mathfrak{F}})$ so that ξ_k, ξ_l are independent for $k \neq l$. Therefore, "smooth" Brownian motions can be simulated by setting $x_t^{K, \mathfrak{F}} = \sum_{k=1}^K \sqrt{\lambda_k^{\mathfrak{F}}} z_k F_k(t)$ with $(z_k)_{k=1}^K \stackrel{\text{i.i.d.}}{\sim} \mathcal{N}(0, 1)$, $K \geq 1$.

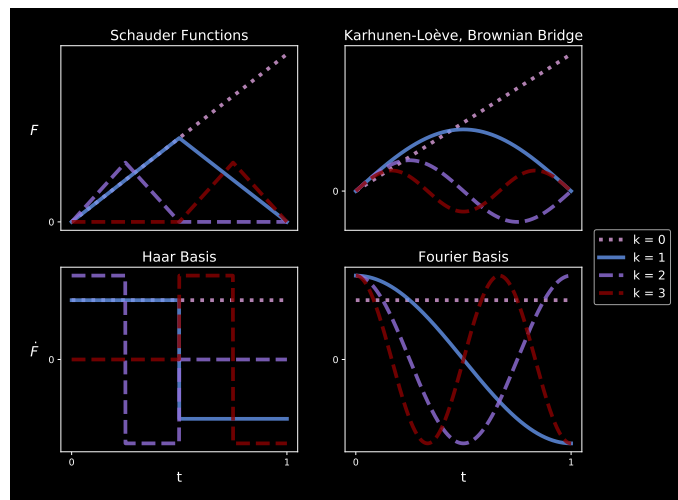
2.2 Lévy-Cieselski Construction

Another Hilbert space is the *Cameron–Martin space*, $\mathcal{R} = \{F \in \Lambda_T \mid dF \ll dt, \dot{F} \in L^2([0, T])\}$ where \dot{F} denotes the time derivative of F . The inner product is $(F, G)_{\mathcal{R}} = (\dot{F}, \dot{G})$, from which (F_k) is an ONB of $\mathcal{R} \iff (\dot{F}_k)$ is an ONB of $L^2([0, T])$ is immediate. If $X^{K, \mathfrak{F}}$ is a projected path with respect to an ONB \mathfrak{F} of \mathcal{R} , then taking derivative gives

$$\dot{x}_t^{K, \mathfrak{F}} = \sum_{k \leq K} (\dot{X}, \dot{F}_k) \dot{F}_k(t) = \sum_{k \leq K} (X, F_k)_{\mathcal{R}} \dot{F}_k(t).$$

We gather that the projection of a path onto \mathcal{R} corresponds to an $L^2([0, T])$ projection of its (possibly generalized) derivative followed by a time integration. When \mathbb{Q} is the Wiener measure, this procedure

Figure 1: Basis functions and derivatives in the Cameron-Martin space.



is often called the *Lévy-Cieselski construction*. With regards to accuracy, we recall the expression for the $L^2(\mathbb{Q} \otimes dt)$ -error,

$$\epsilon^{K, \tilde{\mathfrak{F}}} = \|X - X^{K, \tilde{\mathfrak{F}}}\|_*^2 = \sum_{k, l > K} (\xi_k, \xi_l)_{L^2(\mathbb{Q})} (F_k, F_l)_{L^2([0, T])}.$$

As orthogonal functions in \mathcal{R} need not be orthogonal in $L^2([0, T])$, we cannot in general get rid of the double sum above. However, if \mathbb{Q} is the Wiener measure and \dot{X} the white noise process, then Fubini's theorem gives

$$(\xi_k, \xi_l)_{L^2(\mathbb{Q})} = \int_{[0, T]^2} \underbrace{\mathbb{E}^{\mathbb{Q}}[\dot{x}_s \dot{x}_t]}_{= \delta(t-s)} \dot{F}_k(s) \dot{F}_l(t) ds dt = \int_0^1 \dot{F}_k(t) \dot{F}_l(t) dt = (F_k, F_l)_{\mathcal{R}} = \delta_{kl}.$$

Thus, $\epsilon^{K, \tilde{\mathfrak{F}}} = \sum_{k > K} \|F_k\|^2$. The optimal Cameron-Martin basis would therefore have the fastest decay of its squared norms ($\|F_k\|^2$), assuming the latter are sorted in non-increasing order. We illustrate the Lévy-Cieselski construction with two examples, taking $T = 1$.

Example 2.4. A standard method to prove the existence of Brownian motion follows from the Brownian bridge construction. In short, it consists of a random superposition of triangular functions—the Schauder functions—obtained by integrating the Haar basis on $[0, 1]$,

$$\dot{F}_{k,l}(t) = 2^{k/2} \psi(2^k t - l), \quad 0 \leq l \leq 2^k, \quad t \in [0, 1],$$

with the wavelet $\psi = (-1)^{\mathbb{1}_{[1/2, 1]}}$, $\text{supp}(\psi) = [0, 1]$. It is easily seen that $\dot{F}_{k,l}$ as well as $F_{k,l}$ have support $[l/2^k, (l+1)/2^k]$, the l -th subinterval of the dyadic partition $\Pi_k = \{l/2^k \mid l = 0, \dots, 2^k\}$. The Schauder and Haar functions are illustrated on the left side of Figure 1. Note that the total number of basis functions employed is $K = |\{(k, l) \mid 0 \leq l \leq 2^k, k = 0, \dots, \bar{K}\}| = 2^{\bar{K}+1} - 1$ when considering all functions up to the \bar{K} -th dyadic partition. For Brownian motion, the approximation error is known [4] and equal to $\epsilon^{K, \tilde{\mathfrak{F}}} = \frac{1}{6K}$.

Example 2.5. Let (\dot{F}) be the cosine Fourier ONB, i.e. $\dot{F}_k(t) = \sqrt{2} \cos(\pi k t)$, $t \in [0, 1]$. The anti-derivatives $F_k(t) = \sqrt{2} \frac{\sin(\pi k t)}{\pi k}$ turns out to correspond—up to a factor—to the Karhunen-Loève basis of the Brownian bridge. Indeed, recalling that $\kappa_X(s, t) = s \wedge t - st$ if X is a Brownian bridge, we have for the ONB $\tilde{\mathfrak{F}} = (\tilde{F}_k) = (\pi k F_k)$,

$$(\kappa_X(\cdot, t), \tilde{F}_k) = \sqrt{2} \left[(1-t) \int_0^t s \sin(\pi k s) ds + t \int_t^1 (1-s) \sin(\pi k s) ds \right] = \sqrt{2} \frac{\sin(\pi k t)}{\pi^2 k^2},$$

using integration by parts in the last equality. The eigenvalues are therefore $(\lambda_k^{\tilde{\mathfrak{F}}}) = (\frac{1}{\pi^2 k^2})$. The first elements of $\tilde{\mathfrak{F}}$ and the Fourier cosine ONB are displayed on the right charts of [Figure 1](#). Following the same argument as in [Example 2.3](#), the (minimal) projection error onto K basis functions is approximately equal to $\frac{1}{\pi^2 K}$. This is less than Brownian motion, as little more is known about a Brownian bridge; \mathbb{Q} –almost all trajectories return to the origin.

2.3 Signature and Legendre Polynomials

An alternative characterization of a path is available through the so-called *signature* [16]. Roughly speaking, the signature extract from a path an infinite-dimensional skeleton, where each “bone” contains inherent information. We start off with a few definitions. A *word* is a sequence $\alpha = \alpha_1 \dots \alpha_k$ of letters from the alphabet $\{0, 1\}$. The length of α is denoted by $l(\alpha)$. Moreover, we augment a path $X \in \Lambda$ with the time itself $t \mapsto t$ and write $x_t^0 = t$, $x_t^1 = x_t$. The words $0, 1$ are therefore identified with the time t and path x , respectively. The *signature* in Λ is here seen as a collection of functionals $\mathcal{S} = \{\mathcal{S}_\alpha : \Lambda \rightarrow \mathbb{R}\}$ such that $\mathcal{S}_\emptyset(X_t) \equiv 1$ and

$$\mathcal{S}_\alpha(X_t) = \int_0^t \int_0^{t_k} \dots \int_0^{t_2} \circ dx_{t_1}^{\alpha_1} \dots \circ dx_{t_k}^{\alpha_k}, \quad l(\alpha) = k \geq 1,$$

where \circ indicates Stratonovich integration.³ When referring to a specific path X , we shall call the sequence $(\mathcal{S}_\alpha(X))$ the *signature of X* . If $x_t \in \mathbb{R}^d$ with $d \geq 2$, then the alphabet becomes $\{0, 1, \dots, d\}$ and the signature is defined analogously. The first signature functionals read

$$\begin{aligned} \mathcal{S}_0(X_t) &= \int_0^t dt_1 = t, & \mathcal{S}_1(X_t) &= \int_0^t \circ dx_{t_1} = x_t - x_0, \\ \mathcal{S}_{00}(X_t) &= \int_0^t \int_0^{t_2} dt_1 dt_2 = \frac{t^2}{2}, & \mathcal{S}_{11}(X_t) &= \int_0^t \int_0^{t_2} \circ dx_{t_1} \circ dx_{t_2} = \frac{(x_t - x_0)^2}{2}, \\ \mathcal{S}_{10}(X_t) &= \int_0^t \int_0^{t_2} dx_{t_1} dt_2 = \int_0^t (x_s - x_0) ds, & \mathcal{S}_{01}(X_t) &= \int_0^t \int_0^{t_2} dt_1 dx_{t_2} = \int_0^t s dx_s. \end{aligned}$$

Keeping track of the passage of time is crucial, as the signature would otherwise barely carry information about the path. Indeed, notice that $\mathcal{S}_\alpha(X_t) = \frac{(x_t - x_0)^k}{k!}$ for $\alpha = 1 \dots 1$, $l(\alpha) = k$ (as seen above for $k = 1, 2$) thus only the increment $x_t - x_0$ is known with the alphabet $\{1\}$.

A property of the signature is that it uniquely characterizes a path, up to a equivalence relation: two paths having same signature differ at most by a *tree-like path* [11], a specific type of loop. Hence, extending a path with time not only enriches the signature but also ensures injectivity as $t \rightarrow x_t^0 = t$ is increasing. This gives hope to reconstruct the (unique) path associated to a signature sequence. This was investigated in [9], where the author shows a geometric reconstruction using polygonal approximations for Brownian paths. We propose a simple algorithm, in connection with our discussion on Hilbert projections.⁴ For ease of presentation, assume $x_0 = 0$ and $T = 1$. We first make the following observation.

Lemma 2.6. *Let \overleftarrow{X} denote the time reversed path, i.e. $\overleftarrow{x}_t = x_{1-t}$ and introduce the words $\alpha^{(k)} := 10 \dots 0$, $l(\alpha^{(k)}) = k + 2$, $k \geq 0$. Then $\mathcal{S}_{\alpha^{(k)}}(\overleftarrow{X}_1) = \frac{1}{k!} \mathcal{S}(X, m_k)$ where $m_k(t) = t^k$.*

Proof. First, observe that

$$\mathcal{S}_{\alpha^{(k)}}(X_t) = \int_0^t x_s \frac{(t-s)^k}{k!} ds, \quad \forall t \in [0, 1]. \quad (2.4)$$

³When either the integrand or integrator has bounded variation, the integral is in the Riemann-Stieljes sense and the symbol \circ can be omitted.

⁴I thank Bruno Dupire for suggesting this interesting parallel.

Indeed for fixed $t \in [0, 1]$ and $k = 0$, then $\mathcal{S}_{\alpha^{(0)}}(X_t) = \mathcal{S}_{10}(X_t) = \int_0^t x_s ds$, which is (2.4). Now by induction on $k \geq 1$, uniformly on $[0, t]$,

$$\mathcal{S}_{\alpha^{(k)}}(X_t) = \int_0^t \mathcal{S}_{\alpha^{(k-1)}}(X_u) du = \int_0^t \int_0^u x_s \frac{(u-s)^{k-1}}{(k-1)!} ds du = \int_0^t x_s \frac{(t-s)^k}{k!} ds.$$

Now taking $t = 1$ and \overleftarrow{X} instead of X , we get $\mathcal{S}_{\alpha^{(k)}}(\overleftarrow{X}_1) = \int_0^1 \overleftarrow{x}_t \frac{(1-t)^k}{k!} dt = \frac{1}{k!}(x, m_k)$. \square

Essentially, Lemma 2.6 states that the knowledge of $(\mathcal{S}_{\alpha^{(k)}}(\overleftarrow{X}_1))_{k \geq 0}$ is equivalent to the knowledge of the inner products of the path with the monomials. Since also

$$\mathcal{S}_{\alpha^{(k)}}(\overleftarrow{X}_1) = (-1)^k \int_0^1 x_t \frac{((1-t)-1)^k}{k!} dt = \sum_{j=0}^k \mathcal{S}_{\alpha^{(j)}}(X_1) \frac{(-1)^j}{(k-j)!},$$

the coefficients $(X, m_k)_{k \geq 0}$ can be retrieved from $(\mathcal{S}_{\alpha^{(k)}}(X_1))_{k \geq 0}$ as well. To fall within the context of orthonormal projection, we transform the monomials into the (unique) polynomial ONB of $L^2([0, 1])$. Let (p_k) be the Legendre polynomials [22], forming an orthogonal basis of $L^2([-1, 1])$. Then consider the *shifted Legendre polynomials*, $q_k(t) = p_k(2t - 1)$, $t \in [0, 1]$. We write

$$q_k(t) = \sum_{j \leq k} a_{k,j} t^j, \quad a_{k,j} = (-1)^{k+j} \binom{k}{j} \binom{k+j}{j},$$

with coefficients derived for instance from *Rodrigues' formula* [22, Section 4.3]. The standardization $F_k := \frac{q_k}{\|q_k\|} = \sqrt{2k+1} q_k$ makes $\mathfrak{F} = (F_k)$ an ONB of $L^2([0, 1])$. This leads us to the following result.

Proposition 2.7. *If $b_{k,j} := \sqrt{2k+1} j! a_{k,j}$ and $G_j(t) := \sum_{k=j}^K b_{k,j} F_k(t)$, then*

$$x_t^{K, \mathfrak{F}} = \sum_{k \leq K} \xi_k F_k(t) = \sum_{j \leq K} \mathcal{S}_{\alpha^{(j)}}(\overleftarrow{X}_1) G_j(t). \quad (2.5)$$

Proof. First, note that $(X, F_k) = \sum_{j \leq k} a_{k,j} (X, m_j)$. Using Lemma 2.6, we obtain $\xi_k = \sum_{j \leq k} b_{k,j} \mathcal{S}_{\alpha^{(j)}}(\overleftarrow{X}_1)$. Hence, $x_t^{K, \mathfrak{F}} = \sum_{j \leq K} \mathcal{S}_{\alpha^{(j)}}(\overleftarrow{X}_1) G_j(t)$ with (G_j) as in the statement. \square

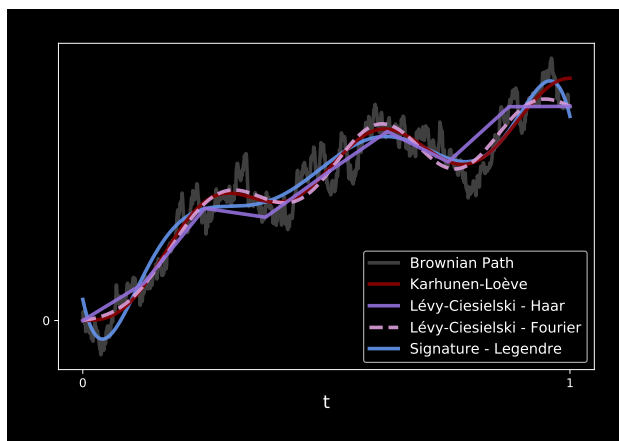
In summary, the signature elements $(\mathcal{S}_{\alpha^{(k)}})_{k \leq K}$ generate the $L^2([0, 1])$ products of the path with the monomials—and in turn, with the Legendre polynomials—from which the projected path $X^{K, \mathfrak{F}}$ becomes available. We can therefore retrieve X by letting $K \rightarrow \infty$. Note that this reconstruction works for multi-dimensional paths as well, as we can apply the procedure to each component $i = 1, \dots, d$ with the words $\alpha^{(i,k)} := i0 \dots 0$, $l(\alpha^{(i,k)}) = k + 2$, $k \geq 0$. We finish this section by computing the projection error of (2.5) when X is Brownian motion. Recalling that $\kappa_X(s, t) = s \wedge t$, a simple calculation gives

$$\lambda_k^{\mathfrak{F}} = \mathbb{E}^{\mathbb{Q}}[\xi_k^2] = 2 \int_0^1 \int_0^t s F_k(s) ds F_k(t) dt = 2(2k+1) \sum_{i,j \leq k} \frac{a_{k,j} a_{k,i}}{(j+2)(i+j+3)}.$$

The first values are given by $(\lambda_k^{\mathfrak{F}})_{k=0}^3 = (\frac{1}{3}, \frac{1}{10}, \frac{1}{42}, \frac{1}{90})$ from which we conjecture that $\lambda_k^{\mathfrak{F}} = \frac{1}{(2k+3)(4k-2)}$ for all $k \geq 1$. This is supported by the fact that $\lambda_k^{\mathfrak{F}}$ must be rational numbers as $a_{k,j} \in \mathbb{Z}$ for all k, j and

$$\sum_{k=0}^K \lambda_k^{\mathfrak{F}} = \frac{1}{3} + \frac{1}{8} \sum_{k=1}^K \left(\frac{1}{2k-1} - \frac{1}{2k+3} \right) = \frac{1}{2} - \frac{K+1}{(2K+3)(4K+2)} \xrightarrow{K \uparrow \infty} \frac{1}{2},$$

coinciding with the total variance of Brownian motion on $[0, 1]$. Thus, the approximation error reads $\epsilon^{K, \mathfrak{F}} = \frac{K+1}{(2K+3)(4K+2)} = \mathcal{O}(\frac{1}{8K})$, which is of course larger than the Karhunen-Loève basis but smaller than the

Figure 2: Projected paths with $K = 8$ basis elements.

Brownian Bridge construction (Example 2.4). Note that polynomial ONB's may well be optimal if the approximation criterion is modified. In [8], the authors show that in the weighted Hilbert space $L^2([0, 1], \mu)$, $\mu(dt) = \frac{dt}{t(1-t)}$, the Karhunen-Loève basis of the Brownian bridge is formed by the anti-derivatives of the Legendre polynomials. Although the construction is different, it is also curiously related to the signature elements $(\mathcal{S}_{\alpha^{(k)}})$; see Theorem 2.3 and 2.4 in [8].

Remark 2.8. Note that the approximation in (2.5) may be improved by adding other elements of the signature, especially those that are nonlinear in X , e.g. $\mathcal{S}_{110}(X_t) = \frac{1}{2} \int_0^t x_s^2 ds$. We postpone this discussion to Section 3.3 when projecting running functionals.

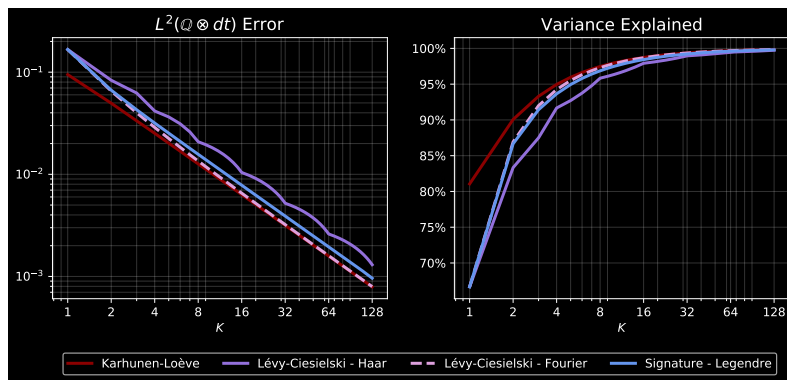
2.4 Numerical Results

We concentrate our experiments on Brownian trajectories. First, we illustrate the path approximations seen earlier (Karhunen-Loève, Lévy-Cieselski, Signature). Figure 2 displays the projections using $K = 8$ basis elements. We naturally notice similarities between the Karhunen-Loève transform and the Lévy-Cieselski construction with Fourier cosines, both obtained by superposing trigonometric functions.

Let us gauge the accuracy of the above approximations for Brownian trajectories, in terms of (i) $\epsilon^{K, \mathfrak{F}}$ and (ii) variance explained $\vartheta^{K, \mathfrak{F}} := \frac{\|X^{K, \mathfrak{F}}\|_*^2}{\|X\|_*^2}$. To compute (i), (ii) and the coefficients $(X, F_k)_{\mathcal{H}}$, we discretize the interval $[0, 1]$ a regular partition made of $N = 10^4$ subintervals. Figure 3 displays the evolution of $\epsilon^{K, \mathfrak{F}}$, $\vartheta^{K, \mathfrak{F}}$ for $K \in \{1, \dots, 128\}$. The Karhunen-Loève expansion clearly dominates the other projections, although being asymptotically equivalent to the Lévy-Cieselski construction with Fourier cosine basis. Besides, the $L^2(\mathbb{Q} \otimes dt)$ convergence of the Brownian bridge construction (Lévy-Cieselski with Haar basis) is non-monotonic. Indeed, a bump appears until a full cycle of the dyadic partition is completed. Lastly, the slopes in the log-log convergence plot (left chart of Figure 3) are roughly equal to -1 . Put differently, the squared approximation error is of order $\mathcal{O}(\frac{1}{K})$, confirming our findings from the above examples.

3 Projection of Functionals

In Section 2, we unveiled two ways to approximate exotic payoffs $\varphi = h \circ f$, namely by projecting the original path X or $Y = f(X)$ directly. If $\pi^{K, \mathfrak{F}}$ denotes as before the projection map onto a Hilbert space

Figure 3: $L^2(\mathbb{Q} \otimes dt)$ error and variance explained.

\mathcal{H} , we can therefore write $\varphi^{K,\mathfrak{F}} := h \circ f^{K,\mathfrak{F}}$, where either $f^{K,\mathfrak{F}} = f \circ \pi^{K,\mathfrak{F}}$ (functional of projected path) or $f^{K,\mathfrak{F}} = \pi^{K,\mathfrak{F}} \circ f$ (projected functional). We shall see in [Section 3.2](#) that the former is suboptimal. Although not so problematic for functionals capturing global features of a path, local path characteristics (e.g. running maximum) will typically be grossly estimated. Indeed, projecting a path first erases most of its microstructure. We thus favor the second option ($f^{K,\mathfrak{F}} = \pi^{K,\mathfrak{F}} \circ f$), which consists of replacing X by Y in (2.1). Let us now focus on $\mathcal{H} = L^2([0, T])$ and demonstrate how to compute the Karhunen-Loève basis of Y .

3.1 Karhunen-Loève Expansion of Functionals

Assume that $Y \in L^2([0, T]) \cap \Lambda_T$ has zero mean (otherwise, see [Remark 2.2](#)). [Theorem 2.1](#) suggests to set \mathfrak{F} equal to the eigenfunctions of $\kappa_Y(s, t) = (y_s, y_t)_{L^2(\mathbb{Q})}$. Optimality comes, however, at the cost of expliciting \mathfrak{F} . We proceed as follows: take a regular partition $\Pi_N = \{t_n = n \delta t \mid n = 0, \dots, N\}$, $\delta t = \frac{T}{N}$ and compute the kernel matrix $\kappa_Y^N = (\kappa_Y(t_n, t_m))_{0 \leq n, m \leq N}$. When κ_Y does not admit a closed-form expression, κ_Y^N is replaced by the sample covariance matrix using simulated paths for Y . The eigenfunctions thus become eigenvectors and solve the systems⁵

$$\sum_{t_n \in \Pi_N} \kappa_Y^N(t_n, t_m) F_k(t_n) \delta t = \lambda_k^{\mathfrak{F}} F_k(t_m), \quad t_m \in \Pi_N, \quad k = 0, \dots, N. \quad (3.1)$$

This is a simple eigenvalue problem so all pairs $(F_k, \lambda_k^{\mathfrak{F}})$ can be computed in one go. Let us proceed with two examples where $T = 1$ and $\mathbb{Q} = \text{Wiener measure}$ throughout.

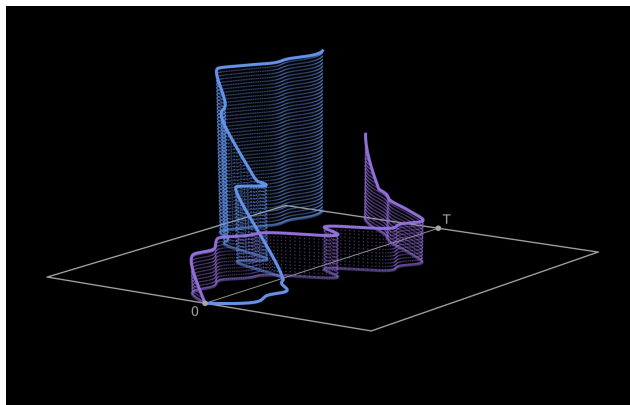
Example 3.1. Consider the time integral and average of a Brownian path, $y_t = f(X_t) = \int_0^t x_s ds$, $\bar{y}_t = \bar{f}(X_t) = \frac{1}{t} \int_0^t f(X_s) ds$. These are clearly centered processes and their covariance kernels can be found explicitly. Starting with Y ,

$$\kappa_Y(s, t) = \left(\int_0^s x_r dr, \int_0^t x_u du \right)_{L^2(\mathbb{Q})} \stackrel{\text{Fubini}}{=} \int_0^s \int_0^t \kappa_X(r, u) dr du.$$

A straightforward calculation gives $\kappa_Y(s, t) = \frac{s^2 t}{2} - \frac{s^3}{6}$, $s \leq t$. The covariance function of the time average follows immediately, namely $\kappa_{\bar{Y}}(s, t) = \frac{s}{2} - \frac{s^2}{6t}$. We display in [Figures 5a](#) and [5b](#) the covariance kernel (top) and first eigenfunctions (bottom) of f and \bar{f} , respectively. The dashed lines in the top panels are the eigenfunctions of the

⁵In (3.1), \sum means that the first and last summand are halved, i.e. the trapezoidal rule is used to compute $(\kappa_Y(\cdot, t), F_k)$. Another approach, known as Nyström's method [19] consists of employing a Gaussian quadrature scheme instead. However, for large N , we haven't observed any improvement and thus favor the more convenient discretization in (3.1).

Figure 4: Running maximum functional for two trajectories.



original (Brownian) path. Note the wider range in the eigenfunctions F_1, F_2 for $\bar{f}(X)$ compared to the integrated path for small t . This might come from the greater fluctuations of the time average at inception.

Example 3.2. Consider the running maximum functional $y_t = f(X_t) = \max_{0 \leq s \leq t} x_s$. Figure 4 provides an illustration in the (t, X, Y) plane. The mean function is in this case non-zero and—using, e.g., the reflection principle—given by $\mathbb{E}^{\mathbb{Q}}[y_t] = \sqrt{\frac{2}{\pi}}t$. The covariance kernel admits an explicit yet complicated expression [3],

$$\kappa_Y(s, t) = \frac{s}{2} + \frac{\sqrt{s(t-s)} - 2\sqrt{st} + t \arcsin(\sqrt{s/t})}{\pi}, \quad s \leq t.$$

Figure 5c displays the covariance kernel (top) and first eigenfunctions (bottom). The latter turns out to be quite close to the eigenfunctions of Brownian motion.

3.2 Numerical Results

Let us compare the $L^2(\mathbb{Q} \otimes dt)$ error $\|Y^{K, \mathfrak{F}} - Y\|_*^2$ in the Brownian case for the two avenues discussed at the beginning of this section. When $Y^{K, \mathfrak{F}} = (f \circ \pi^{K, \mathfrak{F}})(X)$, the error is calculated using Monte Carlo simulations. As in Section 2.4, we choose $T = 1$, $N = 10^4$ and $K \in \{1, \dots, 128\}$. Figure 6 displays the result for the running maximum, integral and average functionals. We also add the Brownian motion itself, corresponding to the identity functional $f(X) = X$. We observe a clear improvement when projecting the transformed path. Moreover, it comes as no surprise that smooth functionals (integral, average) exhibits a faster rate of convergence than the running maximum, highly sensitive to local behaviours of a path.

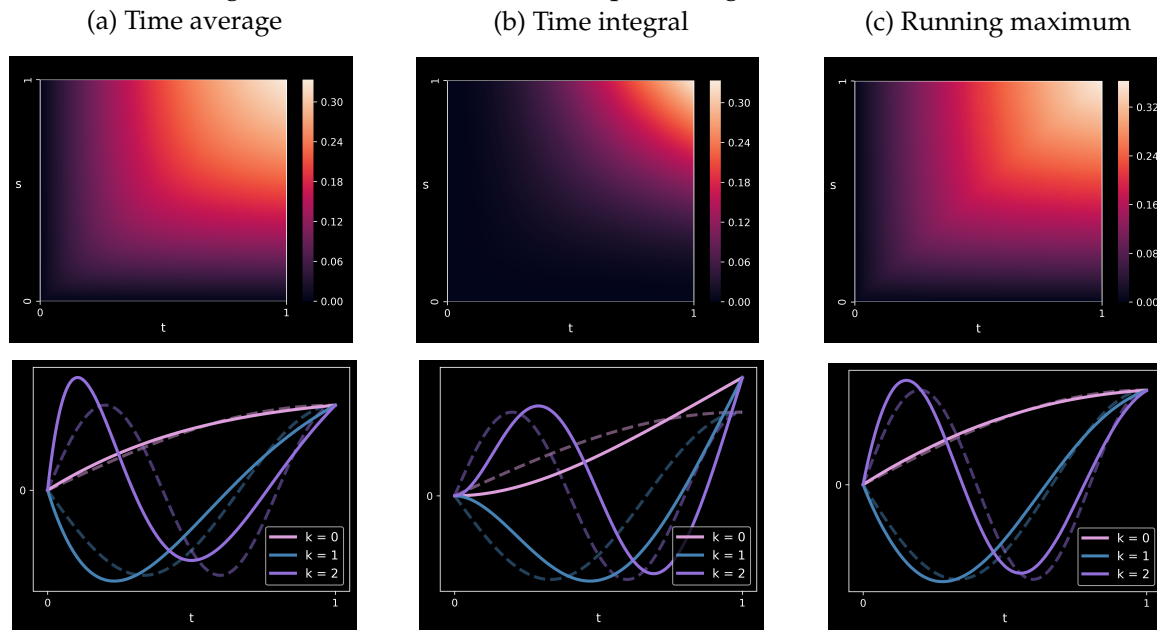
3.3 Discussion: Projection of Functionals using the Signature

Another approximation of $Y = f(X)$ can be obtained by combining signature functionals in a linear fashion. For instance, one can consider all the words of length less than $\bar{K} \in \mathbb{N}$, giving the approximation

$$y_t^{K, \mathcal{S}} := \sum_{l(\alpha) \leq \bar{K}} \xi_{\alpha}^f \mathcal{S}_{\alpha}(X_t), \quad (3.2)$$

with $K = |\{\alpha \mid l(\alpha) \leq \bar{K}\}| = 2^{\bar{K}+1} - 1$. The coefficients ξ_{α}^f may depend on X_0 only and can be calculated by either regressing Y against the signature elements or using a Taylor formula for functionals [14] when f is smooth (in the Dupire sense) and X is a diffusion. In the literature, (3.2) is referred to as *polynomial functional* [14] or *signature payoff* [2, 17] in finance.

Figure 5: Covariance kernels (top) and eigenfunctions (bottom).



Solid lines: transformed path. Dashed lines: Brownian motion.

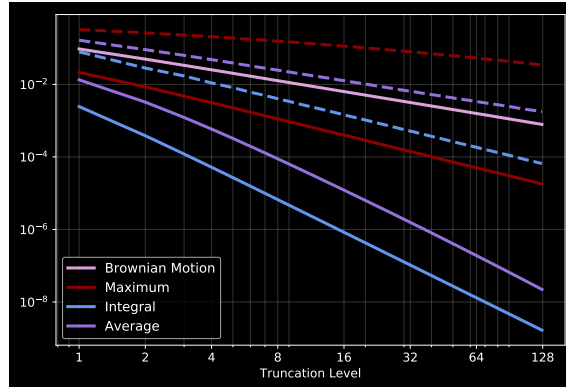
The appeal of such projection comes from the fact that polynomial functionals are dense in the space of continuous functionals restricted to paths of bounded variation; see Theorem 5 in [14]. On the other hand, despite the existence of packages to calculate the signature of discrete time paths (e.g., `iisignature` and `esig` in Python), the projection in (3.2) is still challenging from a computational perspective. Indeed, contrary to the reconstruction in Section 2.3, the signature functionals have to be known at *every* intermediate time. Also, as there is a priori no recipe to select words up to a given length, we must retain all of them so the number of elements doubles every time a layer is added.

4 Applications

We now illustrate the benefits of the Karhunen-Loève expansion on functionals for the pricing of exotic derivatives. We slightly change notations and write W for the coordinate process. The path X now represents the stock price where for simplicity, we employ the Black-Scholes model with zero interest rate. That is, \mathbb{Q} is the Wiener measure and $x_t = x_0 \mathcal{E}_t(\sigma W)$, where $x_0 > 0$ is fixed and \mathcal{E} denotes the stochastic exponential. Notice, however, that our method applies to any dynamics of the underlying.

Let $\mathcal{M} \subseteq \mathbb{R}$, $\mathcal{T} \subseteq [0, T]$ be a finite set of option parameters and maturities, respectively. We seek to approximate the price surface $p : \mathcal{M} \times \mathcal{T} \rightarrow \mathbb{R}$, $p(m, \tau) = \mathbb{E}^{\mathbb{Q}}[\varphi_m(X_\tau)]$, where the payoffs $\varphi_m(X_\tau) = (h_m \circ f)(X_\tau)$ depends on a parameter $m \in \mathcal{M}$. For example, a call option on $Y = f(X)$ is obtained with $h_m^{\text{Call}}(y) := (y - mx_0)^+$ and m is the *moneyness* of the option.

The standard Monte Carlo approach (MC) consists of simulating the underlying path on a partition $\Pi_N = \{0 = t_0 < t_1 < \dots < t_N = T\}$ that contains \mathcal{T} and compute the price as $p^{N,J}(m, \tau) = \frac{1}{J} \sum_{j=1}^J \varphi_m(X_\tau^{N,j})$, $J \in \mathbb{N}$. In contrast, the *Karhunen-Loève Monte Carlo method* (KLMC) samples $Y = f(X)$ directly and computes the price surface using the representation $p(m, \tau) = \mathbb{E}^{\mathbb{Q}}[h_m(y_\tau)]$. We now describe the method in more depth.

Figure 6: $L^2(\mathbb{Q} \otimes dt)$ approximation errors.

Dashed lines: functionals of projected paths.

Solid lines: projected functionals.

Algorithm 4.1 (KLMC)

- **Offline:** Given $f, K, J_{\text{off}}, N_{\text{off}}$
 1. Simulate trajectories $Y^j = (f(X_{t_n}^j))_{t_n \in \Pi_{N_{\text{off}}}}, j = 1, \dots, J_{\text{off}}$
 2. Compute $\kappa_Y^{N_{\text{off}}}$ (closed-form or from the sample (Y^j))
 3. Solve the eigenvalue problem (3.1) to obtain $(\lambda_k^{\tilde{\mathfrak{F}}}, F_k)$
 4. Using (Y^j) , estimate the quantile functions $\Phi_k^{-1}, k \leq K$
 - **Online:** Given $J, \mathcal{M}, \mathcal{T}$
 1. Simulate $\xi_k^j = \Phi_k^{-1}(u_k^j), (u_k^j) \stackrel{i.i.d.}{\sim} U(0, 1), j \leq J, k \leq K$
 2. Compute $y_\tau^{K, \tilde{\mathfrak{F}}, j} = \sum_{k=1}^K \xi_k^j F_k(\tau), \tau \in \mathcal{T}, j \leq J$
 3. Estimate the price surface $p^{K, \tilde{\mathfrak{F}}, J}(m, \tau) := \frac{1}{J} \sum_{j=1}^J h_m(y_\tau^{K, \tilde{\mathfrak{F}}, j})$.
-

4.1 The KLMC Algorithm

We assume for simplicity that Y has zero mean, otherwise minor changes must be made for the KL expansion; see Remark 2.2. First, we simulate trajectories $Y^j = (f(X_{t_n}^j))_{t_n \in \Pi_{N_{\text{off}}}}, j = 1, \dots, J_{\text{off}}$ with $J_{\text{off}}, N_{\text{off}} \in \mathbb{N}$, and compute the eigenfunctions of $\kappa_Y^{N_{\text{off}}}$ as in (3.1). Next, for $k = 1, \dots, K$, we estimate the sample quantile function $\Phi_k^{-1} : [0, 1] \rightarrow \mathbb{R}$ of $\xi_k = (Y, F_k)$ by employing method N°7 in [12]. The coefficients (ξ_k) can thereafter be simulated using inverse transform sampling [7]. Notice that these steps can be done in an offline phase so (Φ_k^{-1}) can be reused for other options contingent upon the functional f ; see Section 2.4.

In the online phase, we simulate $J \in \mathbb{N}$ transformed paths using inverse transform sampling for ξ_k . This gives $y_\tau^{K, \tilde{\mathfrak{F}}, j} = \sum_{k \leq K} \xi_k^j F_k(\tau)$. Finally, the price surface is calculated using Monte Carlo. The procedure is summarized in Algorithm 4.1. It should be noted that although the coefficients (ξ_k) are orthogonal in $L^2(\mathbb{Q})$, they may well be *dependent* when Y is non-Gaussian. While the marginals of $(\xi_k)_{k \leq K}$ are fitted properly, the dependence is omitted as generating dependent random vectors with unknown joint distribution is highly non-trivial. Nevertheless, this simplification doesn't induce a bias in the obtained prices as we shall see in the numerical experiments.

4.2 Numerical Results

First, we build the price surface for Asian and lookback call options, i.e. by choosing $h_m = h_m^{\text{Call}}$ and the running maximum and time average as underlying functional, respectively. Of course, the put option price surface can be retrieved thanks to put-call parity. We also consider Up & Out digital options, that is $f(X_t) = \max_{0 \leq s \leq t} x_s$ and $h_m^{\text{UO}}(y) := \mathbb{1}_{\{y \leq mx_0\}}$. The parameter $m \geq 1$ thus represents the barrier of the option relative to the spot price. We can therefore reuse the quantile functions computed for the lookback call options.

The parameters are $(x_0, \sigma, N_{\text{off}}, J_{\text{off}}, J) = (100, 0.2, 10^3, 2^{17}, 2^{19})$, $T = 1$ year and $\mathcal{T} = \{\frac{1}{52}, \frac{2}{52}, \dots, 1\}$ (weekly maturities). The moneyness and barrier levels are respectively $\mathcal{M}^{\text{Call}} = \{0.75, 0.80, \dots, 1.25\}$ and $\mathcal{M}^{\text{UO}} = \{1.05, 1.10, \dots, 1.50\}$. We assess accuracy in the mean square sense, namely by computing

$$\text{MSE} = \frac{1}{|\mathcal{M}| |\mathcal{T}|} \sum_{(m, \tau) \in \mathcal{M} \times \mathcal{T}} |p^{(\text{B})}(m, \tau) - \hat{p}(m, \tau)|^2.$$

The function \hat{p} is the approximated price and $p^{(\text{B})}$ a benchmark obtained using a standard Monte Carlo with $40 \cdot |\mathcal{T}| = 2080$ time steps and same number of simulations. Table 1 displays the MSE, runtime (online phase) and number of variates per simulated path (K and N for the KLMC and MC method, respectively).⁶ Notice that we increase K, N for the lookback call and Up & Out digital option as the running maximum has a slower rate of $L^2(\mathbb{Q} \otimes dt)$ convergence as seen in Figure 6 for the Brownian case. The KLMC method constantly yields a lower MSE and runtime. For the Asian call option, note that the number of variates per path is less than the number of maturity points and KLMC method, which couldn't be done with the MC method.

Table 1: Mean squared errors and runtime (seconds)

Option	KLMC			MC		
	K	MSE	Time	N	MSE	Time
Asian Call	40	1.50e-04	2.26	52	3.10e-04	2.40
Lookback Call	100	1.15e-02	4.47	4 · 52	1.92e-01	7.05
Up & Out Digital	100	1.80e-04	4.40	4 · 52	1.90e-04	6.88

Conclusion

This paper sheds further light on the approximation of path functionals. After a thorough review of Hilbert projections and a connection with the path signature, we show the power of the Karhunen-Loève expansion to parsimoniously simulate path-dependent payoffs. Further work would include the use of copulas in the KLMC algorithm to capture the dependence between the $L^2([0, T])$ coefficients of the Karhunen-Loève expansion and a performance comparison with signature-based methods.

References

- [1] P. A. Acworth, M. Broadie, and P. Glasserman. *A Comparison of Some Monte Carlo and Quasi Monte Carlo Techniques for Option Pricing*. Springer New York, New York, NY, 1998.

⁶The experiments have been made on a personal computer; see <https://github.com/valentintissot/KLMC> for an implementation. The offline phase takes about 10 seconds per functional.

- [2] I. P. Arribas, C. Salvi, and L. Szpruch. Sig-SDEs model for quantitative finance, 2020.
- [3] O. Bénichou, P. L. Krapivsky, C. Mejía-Monasterio, and G. Oshanin. Temporal correlations of the running maximum of a brownian trajectory. *Phys. Rev. Lett.*, 117:080601, Aug 2016.
- [4] B. Brown, M. Griebel, F. Y. Kuo, and I. H. Sloan. On the expected uniform error of geometric brownian motion approximated by the lévy-ciesielski construction, 2017.
- [5] J. Cao, J. Chen, J. C. Hull, and Z. Poulos. Deep learning for exotic option valuation. *SSRN*, 2021.
- [6] P. Carr and D. Madan. Option valuation using the fast fourier transform. *Journal of Computational Finance*, 2:61–73, 1999.
- [7] L. Devroye. *Non-Uniform Random Variate Generation*. Springer-Verlag, 1986.
- [8] J. Foster, T. Lyons, and H. Oberhauser. An optimal polynomial approximation of brownian motion. *SIAM J. Numer. Anal.*, 58:1393–1421, 2020.
- [9] X. Geng. Reconstruction for the signature of a rough path. *Proceedings of the London Mathematical Society*, 114(3):495–526, 2017.
- [10] R. Ghanem and P. Spanos. *Stochastic Finite Elements: A Spectral Approach*. Springer, New York, NY, 1991.
- [11] B. Hambly and T. Lyons. Uniqueness for the signature of a path of bounded variation and the reduced path group. *Annals of Mathematics*, 171(1):109–167, Mar 2010.
- [12] R. J. Hyndman and Y. Fan. Sample quantiles in statistical packages. *The American Statistician*, 50(4):361–365, 1996.
- [13] K. Karhunen. Über lineare Methoden in der Wahrscheinlichkeitsrechnung. *Annales Academiae scientiarum Fennicae*, 37, 1947.
- [14] C. Litterer and H. Oberhauser. On a Chen-Fliess approximation for diffusion functionals. *Monatshefte für Mathematik*, 175(4):577–593, 2014.
- [15] M. Loève. Fonctions aléatoires du second ordre. *Gauthier Villars*, 1948. Supplement to “Processus Stochastique et Mouvement Brownien” from Paul Lévy.
- [16] T. J. Lyons, M. Caruana, and T. Lévy. *Differential Equations Driven by Rough Paths*. Berlin: Springer, 2007.
- [17] T. J. Lyons, S. Nejad, and I. P. Arribas. Numerical method for model-free pricing of exotic derivatives using rough path signatures. *Applied Mathematical Finance*, 26(6):583–597, 2019.
- [18] J. Mercer. Functions of positive and negative type, and their connection with the theory of integral equations. *Philosophical Transactions of the Royal Society of London.*, 209:415–446, 1909.
- [19] H. J. Reinhardt. *Analysis of approximation methods for differential and integral equations*. Applied mathematical sciences ; v. 57. Springer-Verlag, New York, 1985.
- [20] E. S. Schwartz. The valuation of warrants: Implementing a new approach. *Journal of Financial Economics*, 4(1):79–93, 1977.

- [21] A. Solin and S. Särkkä. Hilbert space methods for reduced-rank gaussian process regression. *Statistics and Computing*, 30, 03 2020.
- [22] G. Szegő. Orthogonal polynomials. *American Mathematical Society*, XXII, 1975. Fourth edition.